ChemComm



COMMUNICATION

View Article Online

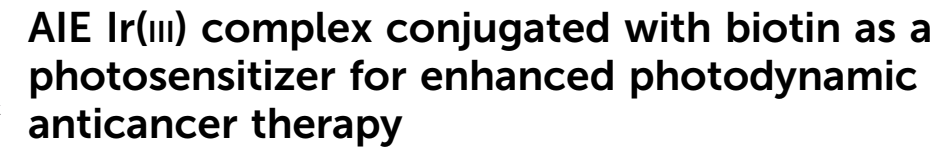


Cite this: DOI: 10.1039/d5cc04806k

Received 20th August 2025, Accepted 3rd October 2025

DOI: 10.1039/d5cc04806k

rsc.li/chemcomm



Zihan Wu,†^a Runlin Wang,†^a Chunguang Shi,^a Dongxia Zhu *\bar *\bar and Martin R. Bryce *\bar *\bar *\bar \bar \bar \bar \bar and \b

The first aggregation induced emission (AIE) Ir(III) complex bearing a biotin-functionalized ligand, Ir-Bio, is reported. Ir-Bio generates type I and type II reactive oxygen species and has an excellent photodynamic therapy effect in cancer cells.

Photodynamic therapy (PDT) is a non-invasive treatment that uses photosensitizers (PSs), light and oxygen (O_2) to selectively combat malignant tumors, vascular diseases and microbial infections. PSs can operate through two main mechanisms: type I and type II. The type II mechanism involves sensitizing singlet oxygen (1O_2) through an energy-transfer process from the excited triplet state of the PS to molecular oxygen in the ground state. PET Regrettably, the highly hypoxic tumor microenvironment significantly limits the effect of type II PDT against tumors. The type I PDT mechanism is based on electron transfer reactions that generate a variety of reactive oxygen species (ROS), such as superoxide ($^{\bullet}O_2^{-}$) and hydroxyl ($^{\bullet}OH$) radicals. Type I PSs decrease reliance on O_2 and demonstrate significant promise in addressing tumor hypoxia.

One of the major challenges of PDT technology is how to obtain sufficient quantities of the PSs in the target tissue for effective treatment. There remains an urgent need for PSs with specific targeting ability. Many Ir(II) complexes have attracted attention as candidate drugs for anticancer therapy due to their unique physiological properties and favorable photophysical attributes, including easy synthesis, structural modifications, strong photostability, and so on. Iridium metal centers can be coordinated with different bidentate ligands through rational design strategies. Therefore, the auxiliary ligands and cyclometalated ligands can be tuned to have different biological functions to

enrich the role of Ir(III) complexes in biological research and therapeutic applications. When the ligands are modified with

targeting molecules, the Ir(III) complex will accumulate in large

quantities in cancer cells, thus improving the antitumor properties. Cancer cells frequently exhibit high levels of tumor-specific

receptors, including biotin receptors that facilitate accelerated growth, proliferation, and survival of the cells. 14-19 Purushotha-

man et al.20 conjugated biotin as a targeting agent to the

chlorophyll derivative TPP, which achieved selective targeting of

the breast cancer cell line MCF-7. However, TPP derivatives may

suffer aggregation-caused quenching (ACQ) of emission in aqu-

eous media, reducing the ROS production. Thus, leveraging the

excellent tumor-targeting ability of biotin and easy modifications

of Ir(III) complexes should be an effective strategy to enhance PDT

In the current work, biotin is linked to the auxiliary ligand to construct the neutral AIE Ir(III) complex **Ir-Bio** with the following desirable features: (i) the ability to generate type I ROS is obtained, (ii) the generation of type II ROS is greatly improved, (iii) the complex effectively accumulates in tumor cells. The PSs **Ir1** (Fig. 1(A)) and **Ir-Bio** (Scheme 1) were obtained by a simple Schiff base reaction in high yields. With the introduction of the

Ir(III) complexes have been reported as PSs, and obtaining AIE Ir(III) complexes as antitumor agents remains a challenge. ^{25,26}

outcomes. However, to date the modification of Ir(m) complexes with biotin for this purpose has not been reported.

Most PSs for PDT are based on organic dyes, including boron dipyrromethene (BODIPY), porphyrin, and their derivatives which have a large planar π -electron system which favours ACQ. The opposite phenomenon, namely aggregation-induced emission (AIE), can enhance fluorescence and ROS generation in an aggregate state through restriction of intramolecular motion (RIM) which prohibits the dissipation of energy. PSs with AIE characteristics overcome the ACQ problem of traditional PSs and have the following advantages: (i) the intersystem crossing (ISC) ability of excited states is significantly improved, (ii) the luminescent quantum efficiency is enhanced, (III) there is high ROS generation. To date, a few AIE

^a Key Laboratory of Nanobiosensing and Nanobioanalysis at Universities of Jilin Province, Department of Chemistry, Northeast Normal University, 5268 Renmin Street, Changchun, Jilin Province 130024, P. R. China. E-mail: zhudx047@nenu.edu.cn

b Department of Chemistry, Durham University, Durham, DH1 3LE, UK. E-mail: m.r.brvce@durham.ac.uk

 $[\]dagger$ The authors contributed equally to the preparation of this work.

Communication ChemComm

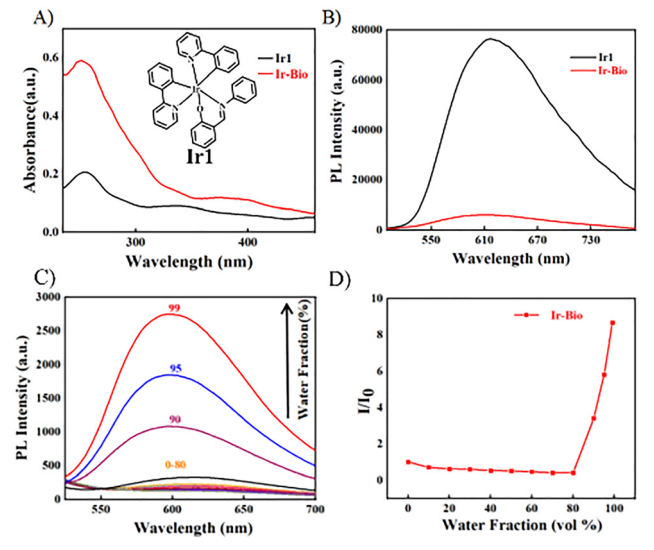
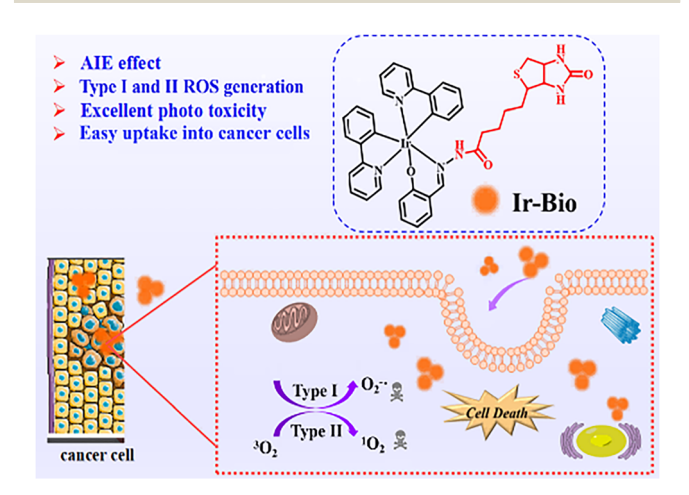


Fig. 1 (A) Ultraviolet (UV)-vis absorption spectra of Ir1/Ir-Bio (10^{-5} M) in CH₃CN/H₂O (v:v=1:9); (B) fluorescence emission spectra, λ_{ex} = 400 nm; (C) fluorescence emission spectra of Ir-Bio in CH₃CN/H₂O mixed solution (10^{-5} M), λ_{ex} = 400 nm; (D) the change of the emission intensity of Ir-Bio in CH₃CN/H₂O with the change of the water concentration.

biotin-assisted ligand, the light absorption and singlet oxygen production capacity of **Ir-Bio** are significantly enhanced compared to **Ir1**. **Ir-Bio** readily accumulates in cells and has high ROS production capacity, which effectively improves the PDT antitumor effect. The work provides a new perspective to address the oxygen deficiency limitation of PSs in PDT, and to improve the uptake of PSs into cancer cells.

The synthetic routes to the ligands L1, L2, and the complexes **Ir1** and **Ir-Bio** (Schemes S1–S5) and corresponding characterization data are provided in the SI with 1H NMR and mass spectra (Fig. S1–S6). The UV-Vis absorption spectra of **Ir1** and **Ir-Bio** at room temperature are shown in Fig. 1(A). Both complexes show strong absorption peaks in the ultraviolet region, and the bands in the range of 250–350 nm are attributed to the $\pi \to \pi^*$ transition centered on the ligands. The



Scheme 1 Structural formula of Ir-Bio and its PDT process.

relatively weak absorption bands in the visible region can be attributed to metal-to-ligand charge transfer transitions, spin-permitted ligand-to-ligand charge transfer transitions, spin-barred metal-to-ligand charge transfer transitions, and spin-barred ligand-to-ligand charge transfer transitions. As shown in Table S1, the absorptive capacity of **Ir-Bio** (ε 58 571 and 12 063 m⁻¹ cm⁻¹) was significantly increased compared to **Ir1** due to the introduction of biotin, indicating high efficiency in photon absorption and utilization. The emission spectra of **Ir1** and **Ir-Bio** were similar, with $\lambda_{\rm max}$ at 610 nm (Fig. 1(B)).

The AIE properties of **Ir1** and **Ir-Bio** were investigated in CH₃CN-H₂O mixtures, where the water content varied from 0 to 99%. As shown in Fig. 1(C), (D) and Fig. S7, **Ir1** and **Ir-Bio** barely emit in pure CH₃CN due to the non-radiative transition process enhanced by molecular vibrations and rotations. As the water content increased to 95%, **Ir1** shows a strong red emission (Fig. S7). **Ir-Bio** showed strongest red emission when the water content increased to 99%. These results establish that **Ir1** and **Ir-Bio** have typical AIE characteristics which will be beneficial to enhance ROS production and therefore improve the effect of PDT.

Efficient ¹O₂ generation is very important for PSs to improve the PDT effect. The ${}^{1}O_{2}$ production of Ir1 and Ir-Bio in DMSO: $H_2O(v:v=1:99)$ was evaluated by monitoring the absorbance changes of indocyanine green (ICG) at 790 nm. For ICG alone, the absorption intensity basically did not change during 210 s of illumination (Fig. 2(A)). Also, the spectra of ICG in the presence of Ir1 or Ir-Bio showed little change without light (Fig. S8). In the cell experiments, PSs need to be irradiated for a relatively long time, and PSs with good light stability are therefore advantageous for PDT. The UV-vis absorption spectra of Ir1 and Ir-Bio did not change during 210 s of illumination which proved their good photostability (Fig. S9). When irradiated with a 405 nm LED lamp for 210 s, the ICG absorption at 790 nm significantly decreased (by > 80%) in the presence of Ir-Bio compared with Ir1 (only about 20%) (Fig. 2(B)-(D)). This data establishes the excellent ¹O₂ generation ability of Ir-Bio. As shown in Fig. 2(E), these data for Ir1 and Ir-Bio conform to the first-order kinetic equation. The higher the slope of the straight line, the stronger the ¹O₂ generation capacity. The Ir-Bio slope (0.00757) is 8.5 times that of Ir1 (0.000888). Using Rose Bengal (RB singlet oxygen production efficiency of 73%) as a reference, the ${}^{1}O_{2}$ quantum yields of Ir1 and Ir-Bio were 17% and 88%, respectively.

Most PSs rely on oxygen to produce singlet oxygen, which is cytotoxic, to achieve cell damage. The oxygen consumption during PDT will further aggravate the oxygen deficiency in the tumor. Therefore, type I PSs that can produce superoxide anion radicals (${}^{\bullet}O_2^{-}$) have a broad application in PDT. As shown in Fig. 2(F), Ir1 (0.1 mM) and 2,2-dimethyl-1-oxido-3,4-dihydropyrrol-1-ium (DMPO as a spin-trapping agent for free radicals) (100 mM) showed no EPR signal in DMSO solution under either dark or light conditions, indicating that Ir1 could not produce superoxide anion radicals. In the dark, Ir-Bio (0.1 mM) and DMPO (100 mM) also did not give any EPR signal. However, when the Ir-Bio and DMPO solution was illuminated, the characteristic superoxide anion radical signal was generated. Therefore, Ir-Bio can realize a type I PDT process and effectively overcome the limitation of

ChemComm Communication

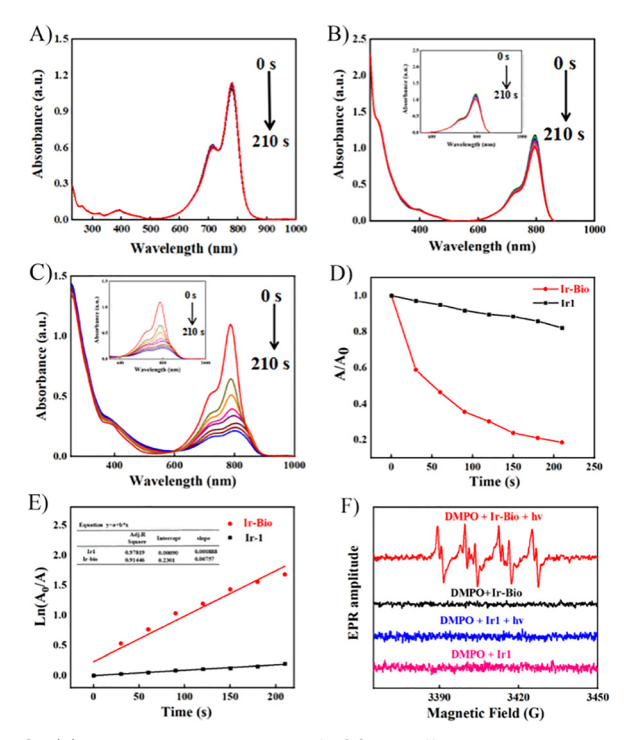


Fig. 2 (A) UV absorption spectra of ICG at different illumination times (405 nm, 20 mW cm $^{-2}$); (B) ICG + **Ir1** + light; (C) ICG + **Ir-Bio** + light; (D) the attenuation curve of ICG at 790 nm when **Ir1** or **Ir-Bio** (18 μM) is present under different illumination times, data in DMSO : H₂O (v: v = 1:99); (E) $^{1}O_{2}$ kinetic generation curve of **Ir1/Ir-Bio**; (F) EPR signals of **Ir1** and **Ir-Bio** (0.1 mM) and DMPO (100 mM) under light and dark conditions in DMSO.

photosensitizer oxygen deficiency in PDT, which opens a new platform for the application of transition metal Ir(III) complex PSs in PDT. In DMSO: H_2O solution (1:99 v:v) Ir1/DMPO and Ir-Bio/DMPO gave no *OH EPR signal under light (405 nm, 20 mW cm⁻¹) or dark, indicating that *OH is not generated in aqueous conditions.

Since Ir1 and Ir-Bio showed excellent ROS production ability in solution, we studied their PDT in vitro by 3-(4,5dimethylthiazol-2-yl)-2,5-diphenyltetrazolium bromide (MTT) assay. As shown in Fig. 3, HeLa cell survival exceeded 80% in dark conditions, even with photosensitizer concentrations up to 50 µM, indicating relatively low dark toxicity of Ir1 and Ir-Bio. However, Ir1 and Ir-Bio showed concentration-dependent phototoxicity with increasing concentration when irradiated by an LED lamp with emission wavelength of 405 nm. When Ir1 concentration reached 50 µM, the cell survival rate was only about 20%. When the **Ir-Bio** concentration was only 25 μ M, the cell survival rate was already reduced to less than 10%. Since Ir1 does not produce superoxide anions, both the Ir1 dark group and the Ir1 light group did not exhibit significant cytotoxicity under hypoxic conditions. Therefore, the phototoxicity of Ir1 under normoxic conditions should be primarily attributed to the type II photodynamic process. The cell survival rate in the irradiated group with Ir-Bio at concentration of 50 µM was less than 40%. This result proved that Ir-Bio could still effectively kill HeLa cells under hypoxic conditions (Fig. S10). Therefore, Ir-Bio has better potential than Ir1 as a PS for cancer treatment.

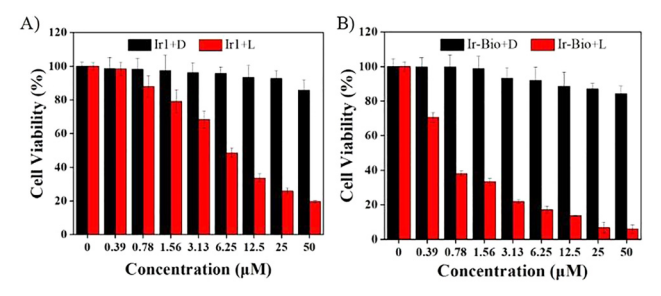


Fig. 3 Survival rate of (A) Ir1 and (B) Ir-Bio-pretreated HeLa cells under dark (D) and illuminated (L) conditions (405 nm, 20 mW cm⁻²).

We further detected and verified ROS production in HeLa cells by using the indicator 2',7'-dichlorofluorescein diacetate (DCFH-DA). As shown in Fig. 4(A), (B) and Fig. S11 in the presence of the PSs Ir1 and Ir-Bio, the intracellular cells showed obvious green fluorescence after light exposure, indicating that DCFH-DA was oxidized to green-emitting DCF by ROS produced by the intracellular photosensitizers. According to the above data Ir1 and Ir-Bio photosensitizers can effectively produce ROS in cells under light.

To observe the live and dead states of cells after the PDT treatment, calcein-AM (live cells, green fluorescence) and propidium iodide (PI) (dead cells, red fluorescence) were costained with HeLa cells to determine the cell death through different fluorescence changes. As shown in Fig. 4(C), (D) and Fig. S12, in the absence of the photosensitizers, green fluorescence was emitted in the cells, and basically no red fluorescence was observed, indicating good cell growth. However, upon illumination at $\lambda_{\rm em}$ 405 nm, the cells showed strong red fluorescence, and basically no green fluorescence. The HeLa cells co-incubated with **Ir-Bio** emitted stronger red fluorescence which indicated that **Ir-Bio** was more enriched in HeLa cells to show better phototoxicity due to the presence of the biotin unit. The results of the live/dead cell staining are consistent with the MTT assay, indicating that **Ir-Bio** is highly enriched and has

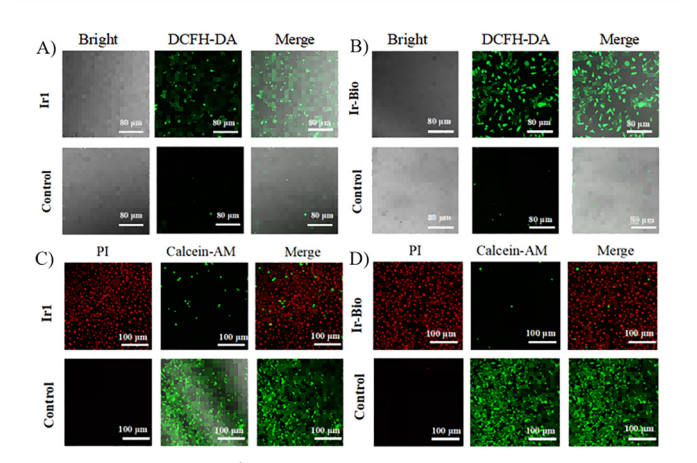


Fig. 4 The intercellular 1 O $_{2}$ capacity was evaluated by DCFH-DA fluorescence intensity after (A) Ir1 and (B) Ir-Bio under darkness and illumination (405 nm, 20 mW cm $^{-2}$); (C) Ir1 was used; (D) fluorescent images of HeLa cells incubated with Ir-Bio (50 μ M).

Communication ChemComm

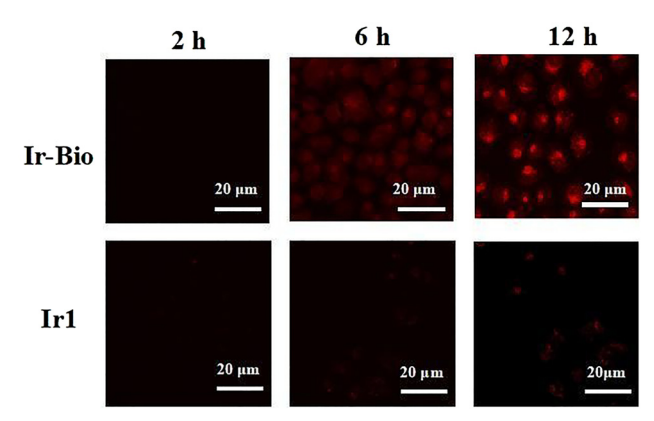


Fig. 5 CLSM images of HeLa cells incubated with **Ir1** or **Ir-Bio** for 2 h, 6 h and 12 h

high ROS production ability in cancer cells, which provides a new molecular strategy to solve the difficulty of transition metal complex photosensitivities in hypoxic PDT.

The uptake of PSs in cells is an important factor affecting the efficacy of tumor therapy. As shown in Fig. 5 and Fig. S13, both Ir1 and Ir-Bio showed time-dependent enhancement of red fluorescence in HeLa cells through confocal laser scanning microscopy (CLSM), indicating that the uptake capacity of both PSs increased gradually over time. In addition, compared with Ir1, it was obvious that HeLa cells incubated with Ir-Bio emitted much stronger red fluorescence for the same incubation time. Furthermore, the uptake ability of A549 cells for the two photosensitizers (Ir1 and Ir-Bio) was measured (Fig. S14 and S15).

After 6 hours of co-incubation with **Ir-Bio**, red fluorescence was emitted within the cells indicating that **Ir-Bio** was effectively internalized by the cells due to stronger uptake of biotin-conjugated ligands, compared with **Ir1**, which would contribute to better PDT killing of cancer cells by **Ir-Bio**. Furthermore, to verify that the uptake is receptor-specifically mediated, we performed a binding assay by incubating HeLa cells with free biotin. After incubating with free biotin for one hour, **Ir-Bio** was added for further incubation. It is notable that no red fluorescence was observed even after 6 hours of co-incubation. This is attributed to the complete binding of the free biotin to the over-expressed biotin receptor on the surface of the HLla cells (Fig. S16 and S17).

In summary, the significance of this work stems from the rational design of an Ir(III) complex bearing biotin functionality on the ancillary ligand. Specifically: (i) **Ir-Bio** has an excellent AIE effect; (ii) **Ir-Bio** achieves type I and type II PDT, and (III) the biotin ligand is beneficial to internalization of the Ir(III) complex by HeLa cells. Overall, this work provides an effective and versatile strategy for improving the PDT effect of Ir(III) complex photosensitizers under hypoxic conditions. Future work will address ligand design for obtaining longer wavelength absorption in **Ir-Bio** complex PSs.

This work was supported by NSFC (no. 52473167), the Key Scientific and Technological Project of Jilin Province (20240402036GH), the Development and Reform Commission of Jilin Province (2024C017-4). M. R. B. thanks EPSRC (UK) grant EP/L02621X/1 for funding.

Conflicts of interest

There are no conflicts to declare.

Data availability

The data associated with this article are available in the manuscript and supplementary information (SI). Supplementary information: experimental details, supporting figures and tables. See DOI: https://doi.org/10.1039/d5cc04806k.

Notes and references

- 1 Z. Zhou, J. Song, L. Nie and X. Chen, Chem. Soc. Rev., 2016, 45, 6597–6626.
- 2 X. Zhong, X. Wang, J. Li, J. Hu, L. Cheng and X. Yang, Coord. Chem. Rev., 2021, 437, 213828.
- 3 Y. Wan, L.-H. Fu, C. Li, J. Lin and P. Huang, *Adv. Mater.*, 2021, 33, 2103978.
- 4 G. Li, M. Wu, Y. Xu, Q. Wang, J. Liu, X. Zhou, H. Ji, Q. Tang, X. Gu, S. Liu, Y. Qin, L. Wu and Q. Zhao, *Coord. Chem. Rev.*, 2023, 478, 214979.
- 5 D. Zhu, Y. Duo, M. Suo, Y. Zhao, L. Xia, Z. Zheng, Y. Li and B. Z. Tang, Angew. Chem., Int. Ed., 2020, 59, 13836.
- 6 J.-N. Liu, W. Bu and J. Shi, Chem. Rev., 2017, 117, 6160.
- 7 K. Chen, P. He, Z. Wang and B. Z. Tang, ACS Nano, 2021, 15, 7735.
- 8 R. Lin, J. Liu, W. Xu, Z. Liu, X. He, C. Zheng, M. Kang, X. Li, Z. Zhang, H. T. Feng, J. W. Y. Lam, D. Wang, M. Chen and B. Z. Tang, Adv. Mater., 2023, 35, e2303212.
- 9 M. Li, J. Xia, R. Tian, J. Wang, J. Fan, J. Du, S. Long, X. Song, J. W. Foley and X. Peng, J. Am. Chem. Soc., 2018, 140, 14851.
- 10 J. Li, L. Zeng, K. Xiong, T. W. Rees, C. Jin, W. Wu, Y. Chen, L. Jia and H. Chao, *Chem. Commun.*, 2019, 55, 10972–10975.
- 11 D.-Y. Zhang, Y. Zheng, H. Zhang, J.-H. Sun, C.-P. Tan, L. He, W. Zhang, L.-N. Ji and Z.-W. Mao, Adv. Sci., 2018, 5, 1800581.
- 12 L. Zhang, Y. Li, W. Che, D. Zhu, G. Li, Z. Xie, N. Song, S. Liu, B. Z. Tang, X. Liu, Z. Su and M. R. Bryce, Adv. Sci., 2019, 6, 1802050.
- 13 P. Zhang, C. K. Chiu, H. Huang, Y. P. Lam, A. Habtemariam, T. Malcomson, M. J. Paterson, G. J. Clarkson, P. B. O'Connor, H. Chao and P. J. Sadler, *Angew. Chem., Int. Ed.*, 2017, 56, 14898.
- 14 M. Li, J. Xia, R. Tian, J. Wang, J. Fan, J. Du, S. Long, X. Song, J. W. Foley and X. Peng, J. Am. Chem. Soc., 2018, 140, 14851–14859.
- 15 K. H. Gebremedhin, M. Li, F. Gao, B. Gurram, J. Fan, J. Wang, Y. Li and X. Peng, *Dyes Pigm.*, 2019, 170, 107617.
- 16 D. Li, X.-Z. Wang, L.-F. Yang, S.-C. Li, Q.-Y. Hu, X. Li, B.-Y. Zheng, M.-R. Ke and J.-D. Huang, ACS Appl. Mater. Interfaces, 2019, 11, 36435–36443.
- 17 X. Pei, F. Huo, Y. Yue, T. Chen and C. Yin, Sens. Actuators, B, 2020, 304, 127431.
- 18 K. Li, L. Qiu, Q. Liu, G. Lv, X. Zhao, S. Wang and J. Lin, J. Photochem. Photobiol., B, 2017, 174, 243–250.
- 19 C. Wang, Y. Xiu, Y. Zhang, Y. Wang, J. Xu, W. Yu and D. Xing, Nanoscale, 2025, 17, 1812–1873.
- 20 B. Purushothaman, J. Choi, S. Park, J. Lee, A. A. S. Samson, S. Hong and J. M. Song, *J. Mater. Chem. B*, 2019, 7, 65.
- 21 H. He, S. Ji, Y. He, A. Zhu, Y. Zou, Y. Deng, H. Ke, H. Yang, Y. Zhao, Z. Guo and H. Chen, Adv. Mater., 2017, 29, 1606690.
- 22 B. Yu, S. Goel, D. Ni, P. A. Ellison, C. M. Siamof, D. Jiang, L. Cheng, L. Kang, F. Yu, Z. Liu, T. E. Barnhart, Q. He, H. Zhang and W. Cai, *Adv. Mater.*, 2018, 30, 1704934.
- 23 B. Yu, H. Wei, Q. He, C. A. Ferreira, C. J. Kutyreff, D. Ni, Z. T. Rosenkrans, L. Cheng, F. Yu, J. W. Engle, X. Lan and W. B. Cai, Angew. Chem., Int. Ed., 2018, 57, 218.
- 24 L. Liu, C. Li, J. Gong, Y. Zhang, W. Ji, L. Feng, G. Jiang, J. Wang and B. Tang, *Angew. Chem., Int. Ed.*, 2023, 62, e202307776.
- 25 L. Zhang, Y. Li, W. Che, D. Zhu, G. Li, Z. Xie, N. Song, S. Liu, B. Tang, X. Liu, Z. Su and M. R. Bryce, Adv. Sci., 2019, 6, 1802050.
- 26 S. Liu, Y. Pei, Y. Sun, Z. Wang, H. Chen, D. Zhu, M. R. Bryce, B. Tang and Y. Chang, *Aggregate*, 2024, 5, e547.